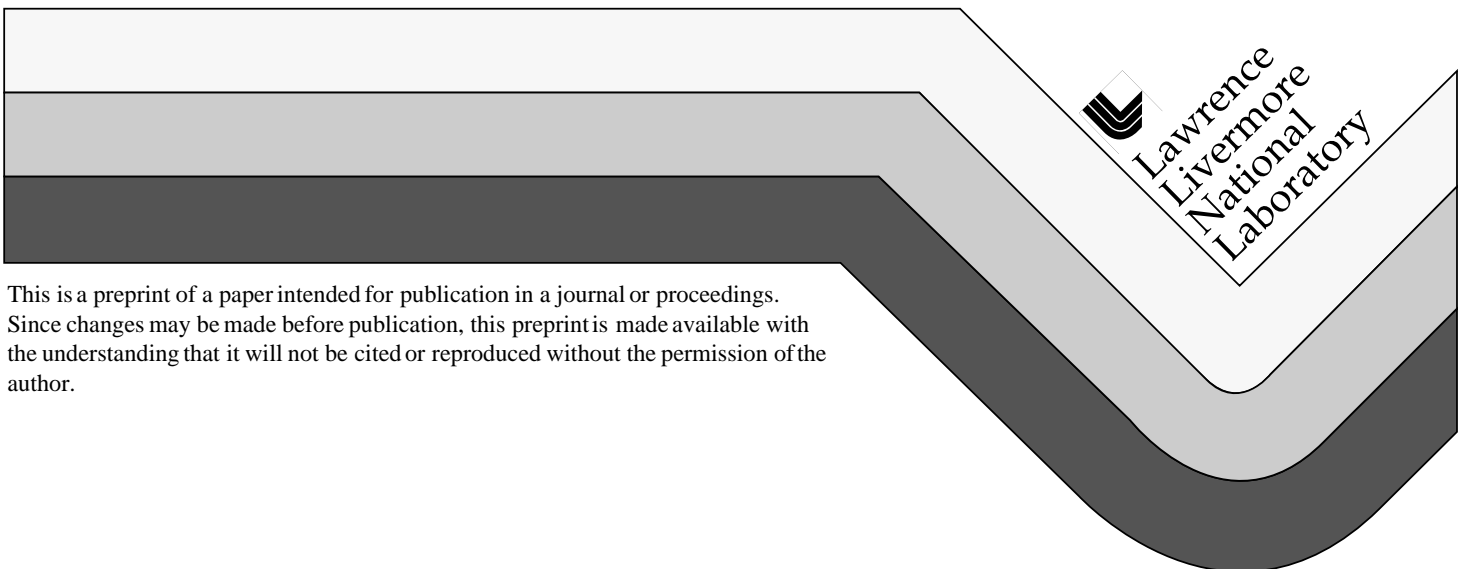


EOS for Critical Slurry and Solution Systems

G. DiPeso
P. Peterson

This paper was prepared for submittal to the
Nuclear Explosives Code Developers Conference
Las Vegas
October 26-30, 1998

October 27, 1998



DISCLAIMER

This document was prepared as an account of work sponsored by an agency of the United States Government. Neither the United States Government nor the University of California nor any of their employees, makes any warranty, express or implied, or assumes any legal liability or responsibility for the accuracy, completeness, or usefulness of any information, apparatus, product, or process disclosed, or represents that its use would not infringe privately owned rights. Reference herein to any specific commercial product, process, or service by trade name, trademark, manufacturer, or otherwise, does not necessarily constitute or imply its endorsement, recommendation, or favoring by the United States Government or the University of California. The views and opinions of authors expressed herein do not necessarily state or reflect those of the United States Government or the University of California, and shall not be used for advertising or product endorsement purposes.

EOS for Critical Slurry and Solution Systems

Gregory DiPeso and Per Peterson
Lawrence Livermore National Laboratory
University of California, Berkeley

In a fire involving fissile material, the mixture of the fissile material ash with fire fighting water may lead to a criticality excursion if there are nearby sumps that permit a critical geometry. The severity of the resulting energy release and pressure pulse is dependent on the rate at which the mixing occurs. To calculate these excursions, a non-equilibrium equation of state for the water ash mixture or slurry is needed that accounts for the thermal non-equilibrium that occurs due to finite heat transfer rates. We are developing the slurry EOS as well as a lumped neutronic and hydrodynamic model to serve as a testing ground for the non-equilibrium EOS before its incorporation into more sophisticated neutronic-hydrodynamics codes. Though the model lacks spatial dependence, it provides estimates of energy release and pressure pulses for various mixture assembly rates. We are also developing a non-equilibrium EOS for critical solution systems in which the fissile material is dissolved in water, which accounts for chemical non-equilibrium due to finite mass transfer rates. In contrast to previously published solution EOS, our solution EOS specifically accounts for mass diffusion of dissolved radiolytic gas to bubble nucleation sites. This EOS was developed to check our overall modeling against published solution excursion experiments and to compare solution excursions with slurry excursions initiated under the same conditions. Preliminary results indicate a good match between solution EOS calculations and experiments involving premixed 60-80 g U/l solutions for both low rate and high rate reactivity insertions. Comparison between slurry and solution calculations for the same composition show comparable energy release and pressure peaks for both low and high rate reactivity insertions with the slurry releasing less energy but generating more pressure than the solution for the amount of energy released. Calculations more appropriate to actual fire fighting scenarios will also be presented. (U)

Keywords: criticality excursion, EOS, mixtures,

Introduction

This report summarizes the status of code development for a coupled neutronic hydrodynamic model needed to calculate output of a criticality excursion in a slurry of water and fissile ash. Such a slurry may be a result of a fire involving nuclear weapons. One scenario involves high pressure fire fighting hoses aimed at fissile ashes in a sump. The water could stir up the ashes and the slurry could reach a critical configuration if there is sufficient ash mass and the sump is of the right size and shape for the given ash mass. Another scenario involves the ash being sloshed into or raining down into a sump already filled with water. The latter scenario would reach a critical configuration over a longer time scale releasing less energy, but both scenarios could result in steam explosions similar to those that can occur when molten metals are quenched in water.

For a specific weapon system, the probability of a fire releasing fissile materials is at least on the same order as the probability assessed for an accidental high explosive violent reaction (HEVR) (Speed, 1998). The HEVR probability assessment is confined to the weapon itself, but for fire fighting scenarios, an assessment also involves a multitude of variables including fire fighting procedures, accident location and type, and the amount of ash release. Assigning probabilities to these variables is difficult since, fortunately, there is little real world data.

As with most risk assessments, one may ask the need to analyze the consequences of events that occur with such small and tenuously determined probabilities. Only consequences that are disastrous merit such analysis. The possibility of a supercritical configuration of fissile ash and fire fighting water generating tens to hundreds of pounds of yield certainly qualifies as disastrous. Even a steam explosion driven by one to a few pounds of yield spreading the radioactive ash beyond the accident site, though a milder consequence, has implications for the personnel in the area. Finally, much effort has already been devoted to assessment of safety concerns that occur with probabilities on the same order or less than that of fissile ash release during a fire and it seems logical to put some effort into this safety concern as well.

Previous efforts to calculate slurry yield have been done by analytic methods (Kruger, 1993). The analysis showed the possibility of 100s of pounds of HE equivalent yield for the high pressure fire hose scenario. One caveat to this analysis was that a neutronic hydrodynamic code be developed to improve the yield estimate. There are coupled neutronic-hydrodynamic codes specializing in criticality excursions in solutions of fissile material (Kimpland and Kornreich, 1996). Furthermore, an ASCI redevelopment of neutronic-hydrodynamic design codes is underway and these codes could conceivably be brought to bear on this problem. What is missing is an appropriate slurry non-equilibrium equation of state, that allows the pressure in the slurry mixture to be calculated as a function of the density and transient fission energy release history. Non-equilibrium effects must be considered due to the nonuniform temperature and gas-concentration distributions that can exist during rapid transients. Development of this non-equilibrium equation of state is the initial focus of our code development effort. This non-equilibrium equation of state could then be incorporated into an existing neutronic-hydrodynamic code.

Most, if not all, of the criticality excursion experience is from fissile solutions, rather than particulate slurries, because solutions commonly occur in nuclear fuel reprocessing activities and thus have been studied experimentally (Mee, et al., 1988, Lecorche and Seale, 1973, Babry, 1987). To demonstrate the difference between fissile slurries and fissile solutions, a non-equilibrium equation of state for a fissile solution was also developed, that accounts for the non-uniform radiolytic gas distribution that occurs in solutions during rapid fission heating transients. Equations of state for fissile solutions previously developed (Kimpland and Kornreich, 1996) do not specifically account for mass diffusion driven bubble growth which leads to system volumetric expansion and subsequent excursion shutdown.

We show a significant difference between solutions and slurries containing the same concentrations of fissile material undergoing the same assembly conditions. Furthermore, the solution results agree reasonably well with fissile solution experiments (Lecorche and Seale, 1973, Babry, 1987) modulo some fit parameters. Similar validation for the slurry equation of state would require slurry experiments. Experiments involving hot metal and ceramic particles dumped into water have been conducted to check the PM-Alpha (Angelini, et al., 1995) two-phase heat transfer code to study the dynamics of steam explosions (Theofanous, et al., 1997). We use the same heat transfer coefficients as the PM-Alpha code for our slurry equation of state and could in principle use the same experiments to check our EOS, recognizing that our zero-dimensional hydrodynamics model provides lower resolution of the highly multi-dimensional hydrodynamic response than the multi-dimensional, multi-phase codes which have been developed specifically to model steam explosions.

To test our EOS, we constructed a zero-dimensional, lumped neutronics-hydrodynamics model. Lumped neutronics is provided by the point kinetics equations (Lutz, 1985). Lumped hydrodynamics is done by assuming a spatially constant density of fluid material, either slurry or solution. For a cylindrical geometry with axial variation in the fluid velocity and pressure, volume averages of the mass and momentum conservation equations provide ordinary differential

equations for the density advance as a function of the spatially averaged or system pressure. The system pressure, density, and fission heating history are related by the EOS. The hydrodynamics treatment is admittedly crude but is useful for demonstrating slurry versus solution differences and providing a framework for how the non-equilibrium EOS can couple into a multidimensional coupled neutronics-hydrodynamics code. The code organization is shown in Fig. 1.

The plan of the report is as follows. We first present the lumped neutronic-hydrodynamic model. We then present the slurry and solution equations of state. Next, we show the comparison between solution calculations and experiment. In this section, we also show the consequences if the experiments had been carried out with a slurry instead of a solution. In the next section, we show slurry excursions for rapid assemblies

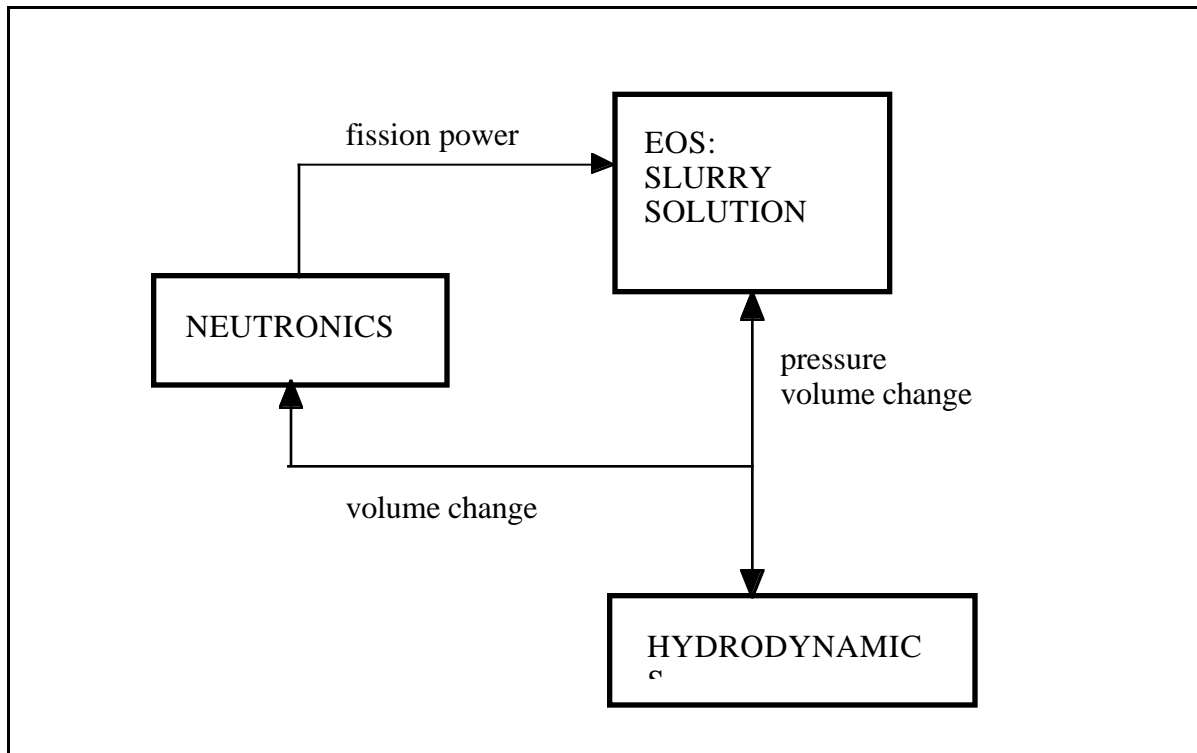


Figure 1: Code layout

during high-pressure fire hose scenarios. Finally, in the last section, we outline code development plans for the next fiscal year.

Lumped Neutronics and Hydrodynamics

Neutronics. We use a point kinetic model for the neutronics calculations. This model is described in great detail by Lutz who also provides data for delayed neutron precursors (Lutz, 1985). The point kinetic model is essentially the time varying portion of the neutron diffusion equation in an assembly. The spatial variation is given by the eigenvalue of the diffusion equation but we use the time varying value as the constant neutron density in our lumped model. This, in conjunction with a lumped hydrodynamics model, is sufficient for an EOS testbed.

The neutron density is given by the equation

$$\dot{n} = \frac{q - \beta}{l} n + \sum_{i=1}^6 \lambda_i c_i + \frac{SM_{OY}}{V_A} \quad (1)$$

where the dot signifies a derivative with respect to time, n is the neutron density, q is the reactivity, l is the neutron lifetime, β is the fraction of delayed neutrons, i.e. the fraction of neutrons due to the decay of certain fission products called delayed neutron precursors, λ_i is the i th precursor decay rate, c_i is the i th precursor density, S is the source neutron production rate per unit mass of oralloy fuel, M_{OY} is the fuel mass and V_A is the assembly volume.

The precursors are binned into $i=1,6$ groups based on decay rate. The i th precursor density is given by

$$\dot{c}_i = \frac{f_i \beta}{l} n - \lambda_i c_i \quad (2)$$

where f_i is the ratio of delayed neutrons from the decay of the i th precursor to the total number of delayed neutrons. The values of λ_i and f_i have been tabulated by Lutz (Lutz, 1985). For fissile solutions, $\beta \approx 0.008$ is used for oralloy solutions (Mee, et al., 1988, Kornreich, 1993).

The lifetime is given by

$$l = \frac{1}{v v_t \Sigma_f} \quad (3)$$

where $v \approx 2.4$ is the average number of neutrons generated per fission, $v_t = 2200$ m/s is the thermal neutron velocity and Σ_f is the macroscopic fission cross section for oralloy given by

$$\Sigma_f = \frac{6 \times 10^{23} M_{OY}}{V_A} \left[\frac{0.93 \sigma_{f235}}{A_{235}} + \frac{0.07 \sigma_{f238}}{A_{238}} \right] \quad (4)$$

The microscopic fission cross sections for thermal neutrons are $\sigma_{f235} = 577$ barns = 577×10^{-28} m² and $\sigma_{f238} = 4.95$ barns = 4.95×10^{-28} m² (Duderstadt and Hamilton, 1976). The atomic numbers are $A_{235} = 0.235$ kg/mole and $A_{238} = 0.238$ kg/mole.

Fission leads directly to power production as the assembly goes beyond critical. The total power in the assembly is given by

$$W_A = V_A \epsilon v_T \Sigma_f n \quad (5)$$

where $\epsilon = 2.88 \times 10^{-11}$ J/fission.

The reactivity is defined as

$$q = \frac{k - 1}{k} \quad (6)$$

where k is the assembly criticality which is a function of assembly composition and geometry. Once the excursion starts, reactivity is written as the sum of an insertion term due to mechanisms

outside the reactor, e.g. insertion or withdrawal of a control rod by a reactor operator, addition of water to a sump containing fissile ash, and feedback terms due to the reaction of the assembly, e.g. fission heating leading to expansion bringing the assembly away from criticality. The feedback coefficients for fissile solutions have been tabulated only for specific compositions pertaining to actual fissile solution criticality experiments (Kimpland and Kornreich, 1996, Kornreich, 1993).

$$\dot{q} = \dot{q}_I t - \alpha_V V_V - \alpha_E \Delta V_{w,E} \quad (7)$$

where $d/dt q_I$ is the insertion rate, α_V is the feedback due to void formation by gas bubbles or vapor clouds around particulates, and α_E is the feedback due to thermal expansion of liquid water. V_V is the void volume and $\Delta V_{w,E}$ is the volume change in the water due to thermal expansion alone. The feedback coefficients are strongly dependent on the concentration level of the uranium in the solution. Kimpland and Kornreich calculate feedback coefficients for only low concentrations (<100 g/l). Kornreich, in an earlier paper calculated a table of feedback coefficients at higher concentrations but without a void coefficient. Additional feedback mechanisms, e.g. Doppler broadening of neutron cross section resonances by temperature increase are not considered here but are presumably incorporated in the more sophisticated neutronic-hydrodynamic models for which the slurry EOS is being developed.

Before the excursion, the insertion rate can be found from the time derivative of Eq. (6) and the criticality given by the modified one energy group neutron criticality expression

$$k = \frac{k_\infty}{1 + M^2 B^2} \quad (8)$$

where k_∞ is the criticality in an infinite medium, M is the migration length which accounts for both the thermal neutron diffusion length and the length required for a fission neutron born at speeds greater than thermal to collide with atomic constituents of water and slow down to thermal speeds, and B is the geometrical buckling. Equation (8) is the eigenvalue of the neutron diffusion equation. For cylindrical geometry with neutron reflection only at the bottom, as in the CRAC experiments (Lecorche and Seale, 1973), the buckling is given by

$$B^2 = \left(\frac{2.405}{R_A + \lambda_U} \right)^2 + \left(\frac{\pi}{H_A + \lambda_U + \lambda_R} \right)^2 \quad (9)$$

where λ_U and λ_R are the unreflected and reflected diffusion boundary extrapolation lengths and H_A and R_A are the assembly height and radius which are related to the assembly volume by $V_A = \pi R_A^2 H_A$. For CRAC, the assembly radius is fixed. The values for k_∞ , M^2 , and λ_U and λ_R have been tabulated by Mee (Mee, et al., 1988) for concentrations of uranyl nitrate in water ranging from a few grams per liter to several hundred grams per liter. We use the same tabulated quantities for our comparisons to SILENE which is actually an annular reactor with the same uranyl nitrate solution.

Because the source term $S M_{OY}$ in Eq. (1) is weak in or alloy, it is possible that a fission chain reaction is not sustained even for $q > \beta$ (reactivity beyond prompt critical) because of statistical fluctuations. For plutonium systems, such considerations do not arise, but here we are focusing

solely on oralloy systems. The fluctuation effect causes the average initiation time for the point kinetics equations to be greater than the time at which the assembly reaches prompt critical. The initiation time is given by (Lutz, 1985)

$$t_I \cong t_p + \delta \sqrt{\frac{\pi}{2 \dot{q} SM_{Or}}} \quad (10)$$

where t_p is the time at which $q = \beta$ (prompt critical) and δ signifies that the square root term is an average delay with the actual value fluctuating. If $\delta = 0$, initiation is at prompt critical. If $\delta = 2$, the maximum observed delay is achieved. Typically, $\delta \approx 1$ and δ is an input variable for our testbed. Note that if S were larger or larger oralloy masses were involved or if the reactivity insertion rate is very fast, the delay time is diminished. The initial conditions for Eqs. (1) and (2) are then $n(t_I) = c_I(t_I) = 0$.

The significance of this delay is that larger reactivities are built up before a fission chain is initiated. This translates to a faster fission power rise time and greater energy release before reactivity decrease and criticality excursion shut down by volume expansion can occur. Note that for reactors at an initially low steady state power, the delay time is zero even for oralloy fuel since the system has already been brought under control. The initial conditions $n(t_I) = c_I(t_I) = 0$ are not strictly correct but are reasonable for large pulses such as the one we model for SILENE.

The system is sent into supercriticality by adding fissile material and/or moderator at a prescribed mass rate. The addition or fill continues while the excursion proceeds. The volume of solution or water/ash slurry increase at a rate equal to the mass addition rate divided by the density. Internal energy is also updated consistently. The fill is done in a separate step from the assembly hydrodynamics as the simulation advances in time. Furthermore, fill volume changes do not contribute to the reactivity feedback. In contrast to CRAC, the SILENE reactor pulse is initiated not by solution addition but by burst rod ejection, but we start the SILENE pulse by solution addition anyway.

If the pressure for the excursion in a solution or slurry could be fixed at some initial background value, e.g. 1 atm, then the EOS would be driven only by fission heating and no assembly hydrodynamics calculation would be required. However, volume production either by radiolytic gas bubble formation or by vaporization causes the solution or slurry to pressurize. Thus a hydrodynamic description is needed.

Hydrodynamics. In a tank with rigid side and bottom surfaces and only axial, i.e. z , motion allowed, the conservation of mass and momentum in the absence of viscosity or external forces can be written

$$\partial_t \rho + \partial_z \rho u_z(z) = 0 \quad (11)$$

$$\rho \partial_t u_z(z) + \rho u_z(z) \partial_z u_z(z) = -\partial_z p(z) \quad (12)$$

where ρ is the fluid density, u_z is the fluid velocity, and p is the local pressure. Note that we specifically indicate the z dependence in the fluid velocity and local pressure. We now assume a spatially constant density and a zero fluid velocity at the bottom of our tank at $z=0$. Integrating Eq. (11) gives

$$u_z(z) = -\frac{z\theta}{\rho} \quad (13)$$

where $\theta \equiv \dot{\rho}$. Substituting this result into Eq. (12) gives

$$p(z) = P_B + \frac{1}{2} \left[\rho \frac{d}{dt} \left(\frac{\theta}{\rho} \right) - \frac{\theta^2}{\rho} \right] (z^2 - H_A^2) \quad (14)$$

where H_A is the assembly height and P_B is the local pressure at $z = H_A$. P_B is the background pressure.

Now we define the system pressure P as the average of the local pressure $p(z)$ over the assembly height or with Eq. (14),

$$\begin{aligned} P &= \frac{1}{H_A} \int_0^{H_A} p(z) dz \\ &= P_B - \frac{H_A^2}{3} \left[\rho \frac{d}{dt} \left(\frac{\theta}{\rho} \right) - \frac{\theta^2}{\rho} \right] \end{aligned} \quad (15)$$

Equation (15) describes a relationship between density time derivatives and the system pressure. The equation may be expressed in a more numerically convenient form as

$$\dot{\rho} = \theta \quad (16)$$

$$\dot{\theta} = \frac{2\theta^2}{\rho} + \frac{3}{H_A^2} (P_B - P) \quad (17)$$

The initial conditions for these equations are $\rho = \rho_1$ and $\theta = 0$. During the hydrodynamic step, Eqs. (16) and (17) are advanced and assuming no mass changes, a volume change is calculated. It is this volume change at system pressure P that must match an EOS calculated volume change also at system pressure P but for some fission heating level. The volume change also produces a change in the assembly height for a given fixed tank radius. If the volume change is an expansion, Eq. (7) indicates a reduction in reactivity which will slowdown and eventually shutdown the criticality excursion.

Equations of State

Solution. When fissions occur in fissile material dissolved in water, the energetic fission products escape the fission site and slow down imparting energy directly into the water. The energy is sufficient to convert water into hydrogen and oxygen gas by radiolysis, but the sensible heat is transferred to the remaining liquid water causing a temperature rise and volume expansion. The volume expansion causes a reduction in reactivity via the second feedback term in Eq. (7). For slow reactivity insertions in a solution assembly, the volume expansion by direct heating is the main shutdown mechanism.

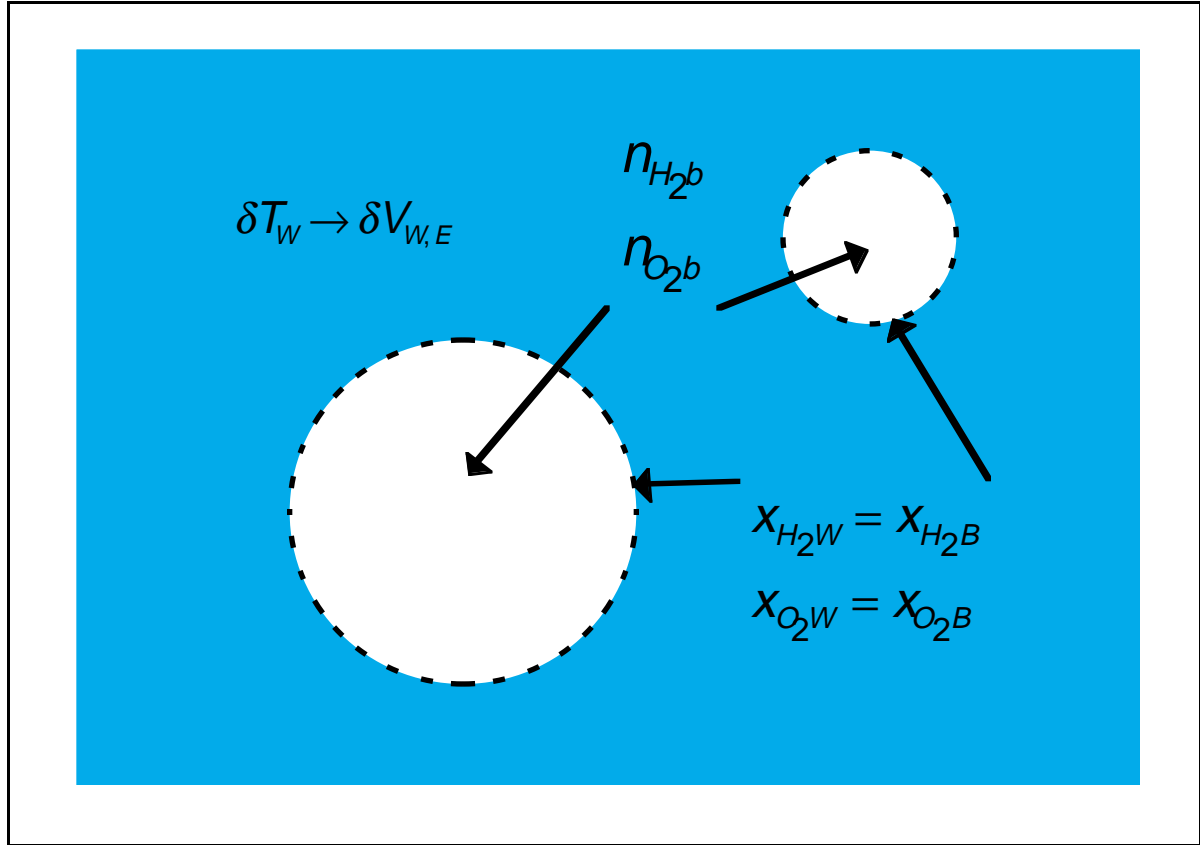


Figure 2a: Physical quantities before gas concentration threshold reached.

The fission products also form nucleation sites for bubble growth. The sites are unstable and collapse with some average lifetime until a threshold concentration of dissolved hydrogen and oxygen gas in the water is reached. Then bubble growth by mass diffusion can occur. These now stable bubbles cause a reduction in reactivity via the first feedback term in Eq. (7). The heat involved still finds its way into the water causing a temperature driven volume expansion but now void growth adds to the reactivity feedback.

Figure 2a shows a schematic of the solution quantities before mass diffusion can occur. The n quantities stand for the number of gas moles inside the nucleation site. The dashed lines encompassing the nucleation sites denotes the sites' instability. The x quantities stand for mole fraction of dissolved gas in the water. The subscript W indicates the mole fraction in the bulk of the water and the subscript B indicates the mole fraction in the water just at the nucleation site interface. Since diffusion has not begun, the mole fractions are initially equal.

We first consider the heating of the liquid water and the volume expansion. In differential form, the energy equation and the liquid water equation of state can be written

$$\delta T_w = \frac{(\delta t W_A - P \delta V_w)}{M_w C_w} \tag{18}$$

$$\delta V_w = V_w \left(\beta_w \delta T_w - \frac{\delta P}{K_w} \right) \tag{19}$$

where M is mass, C is heat capacity, δt is the numerical time step, V is the volume, W_A is the fission power from Eq. (5), δP is the change in system pressure, K is the bulk modulus, and β is the volumetric coefficient of thermal expansion. Note the energy equation accounts for PdV work and the liquid water EOS accounts for pressure changes. The accumulation of δV_w s leads to the $\Delta V_{w,E}$ term in Eq. (7).

The rate of increase of the dissolved gas mole fraction is proportional to the fission power or

$$\dot{x}_{H_2W} = \frac{GW_A}{(\Lambda_{H_2} + 0.5\Lambda_{O_2})n_w} \quad (20)$$

$$\dot{x}_{O_2W} = \frac{GW_A}{2(\Lambda_{H_2} + 0.5\Lambda_{O_2})n_w} \quad (21)$$

where G is the mass of radiolytic gas generated per unit of fission energy (kg/J), Λ is the mass per mole atomic number (kg/mole), and $n_w = M_w / \Lambda_w$ is the moles of water in the assembly.

Since diffusion has not yet begun, the advance of the mole fraction of radiolytic gas at the nucleation site interface is also given by Eqs. (20) and (21). Although the nucleation sites are unstable, during their brief existence, they contain radiolytic gas at a partial pressure proportional to the interface mole fraction or

$$P_{H_2} = \Gamma_{H_2} x_{H_2W} \quad (22)$$

$$P_{O_2} = \Gamma_{O_2} x_{O_2W} \quad (23)$$

The Γ are the Henry's law constants for the gas species dissolved in water. If we assume the nucleation site gas is at the water saturation temperature, then the Clapeyron equation can be used to get the nucleation site gas temperature or

$$T_b = T_{ref} \left[1 - \chi \log \left(\frac{P_{H_2} + P_{O_2}}{P_{ref}} \right) \right]^{-1} \quad (24)$$

where for $T_{ref} = 300$ K and $P_{ref} = 0.1$ MPa, $\chi = 0.08$.

The nucleation sites are spherical and have a radius R_{b0} on the order of a hundred nanometers. The number of nucleation sites is directly proportional to the product of the fission rate and the site lifetime or

$$N_b = \frac{2W_A \tau_b}{\varepsilon} \quad (25)$$

where τ_b is the nucleation site lifetime on the order of tens of microseconds. Specific values of R_{b0} and τ_b are correlated (Norman and Spiegler, 1953). For our testbed, the values of R_{b0} and τ_b are

user inputs. The quantities give a *total* volume of gas existing at any given moment in the unstable nucleation sites:

$$V_b = \frac{4\pi}{3} N_b R_{b0}^3 \quad (26)$$

Since the nucleation sites are unstable, this volume does not contribute to reactivity feedback via Eq. (7), but the change in volume contributes to the volume change that must be matched by the hydrodynamics.

With the volume given by Eq. (26), the temperature given by Eq. (24), and the partial pressures given by Eqs. (22) and (23), Dalton's law and the ideal gas law combine to give the mole content at the nucleation sites:

$$n_{H_2b} = \frac{P_{H_2} V_b}{\Omega T_b} \quad (27)$$

$$n_{O_2b} = \frac{P_{O_2} V_b}{\Omega T_b} \quad (28)$$

where $\Omega = 8.315$ J/mole-K.

Mass diffusion and bubble growth start when a sufficient quantity of dissolved gas builds up such that the gas pressure inside the nucleation site, proportional by Henry's law to the interface dissolved gas mole fraction, balances the system pressure and the surface tension forces that collapse the nucleation site. The balance gives the threshold equation for mass diffusion:

$$P_{H_2} + P_{O_2} = P + \frac{2\gamma}{R_{b0}} \quad (29)$$

where γ is the water surface tension. When Eq. (29) is satisfied, N_b from Eq. (25) is frozen at $N_{bb} = W_A(t_b)\tau_b / \varepsilon$ with the assumption that new fission radiolytic gas causes

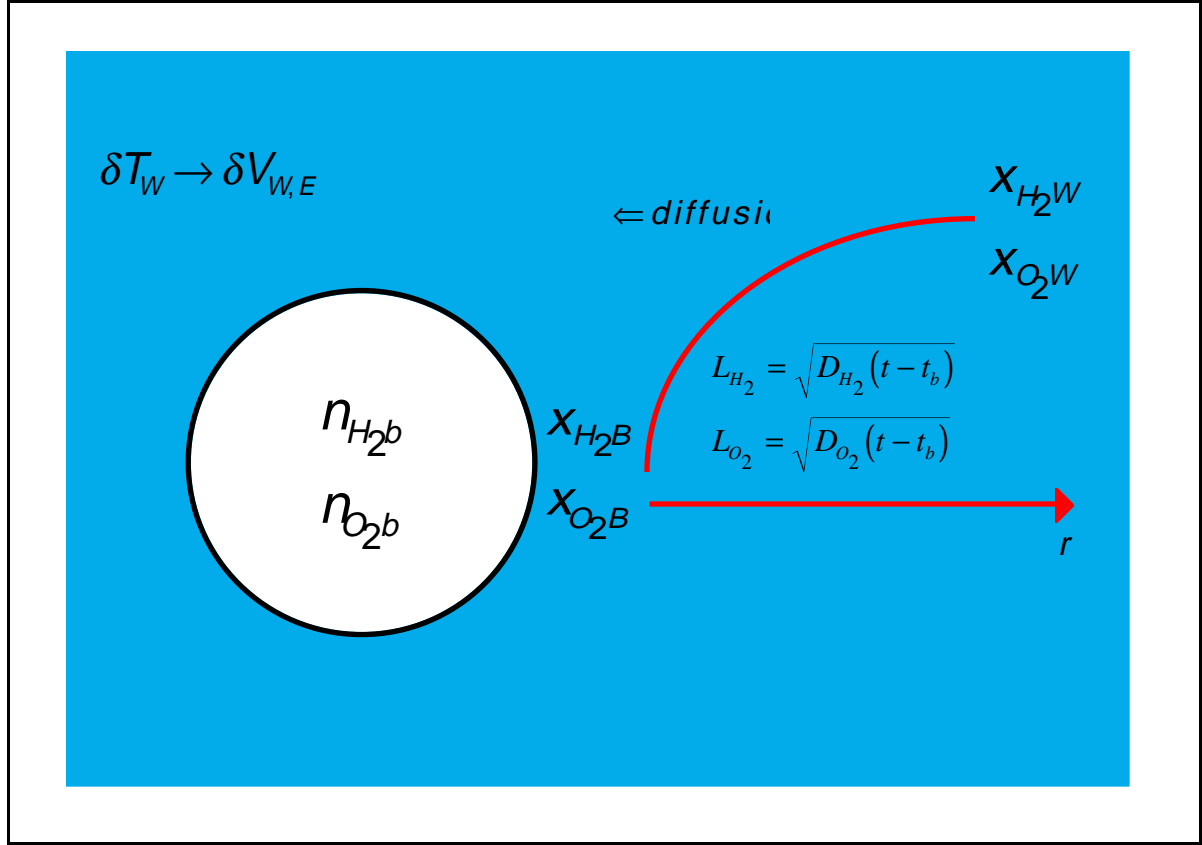


Figure 2b: Physical quantities during mass diffusion.

growth of bubbles with no formation of new nucleation sites, i.e. big bubbles always win over new small bubbles. Equations (27) and (28) give the initial total mole counts for mass diffusion.

The diffusion process quantities are shown in Fig. 2b. The bubble interface is drawn with a solid line to indicate stability. The diffusion is concentration gradient driven. The diffusion lengths L shown in Fig. 2b are a function of the mass diffusion coefficient D and the time $t - t_b$ over which diffusion occurs. t_b is the time at which Eq. (29) is first satisfied. The total mole count is then advanced by $dn/dt = 4\pi R_b^2 N_b D \nabla C$, where C is the moles per cubic meter concentration. Since $\nabla C \approx (n_w / V_w)(x_w - x_b) / L$, the advance for the total mole count is

$$\dot{n}_{H_2b} = 4\pi R_b^2 N_{bb} \frac{n_w}{V_w} \sqrt{\frac{D_{H_2}}{(t-t_b)}} (x_{H_2W} - x_{H_2B}) \quad (30)$$

$$\dot{n}_{O_2b} = 4\pi R_b^2 N_{bb} \frac{n_w}{V_w} \sqrt{\frac{D_{O_2}}{(t-t_b)}} (x_{O_2W} - x_{O_2B}) \quad (31)$$

Note that at $t = t_b$, $x_{H_2W} = x_{H_2B}$ and $x_{O_2W} = x_{O_2B}$, but as $t > t_b$, these quantities also advance in time.

Equations (20) and (21) are modified for $t > t_b$ as

$$x_{H_2w} = \frac{GW_A}{(\Lambda_{H_2} + 0.5\Lambda_{O_2})n_w} - \frac{\dot{n}_{H_2b}}{n_w} \quad (32)$$

$$x_{O_2w} = \frac{GW_A}{2(\Lambda_{H_2} + 0.5\Lambda_{O_2})n_w} - \frac{\dot{n}_{O_2b}}{n_w} \quad (33)$$

Next, the new bubble radius, total bubble volume and bubble gas temperature must be found. Equation (29) is modified for $t > t_b$ as

$$P_{H_2} + P_{O_2} = P + \frac{2\gamma}{R_b} \quad (34)$$

Thus for some system pressure, the total pressure inside a bubble is just a function of the current bubble radius. The temperature inside the bubble can then be given by a modified version of Eq. (24)

$$T_b = T_{ref} \left[1 - \chi \log \left(\frac{P + 2\gamma / R_b}{P_{ref}} \right) \right]^{-1} \quad (35)$$

The total volume of all bubbles is given by a modified version of Eq. (26) as

$$V_b = \frac{4\pi}{3} N_{bb} R_b^3 \quad (36)$$

The ideal gas equation for all bubble gas is

$$(P + 2\gamma / R_b) V_b = (n_{H_2b} + n_{O_2b}) \Omega T_b \quad (37)$$

where the sum of the total mole counts are known from the advance of Eqs. (30) and (31). Here the partial pressure of water vapor is neglected. Equations (35), (36), and (37) are all iterated to find the unknowns R_b , V_b , and T_b .

Equations, (27) and (28) are modified for $t > t_b$ to find the individual gas partial pressures:

$$P_{H_2} = \frac{n_{H_2b} V_b}{\Omega T_b} \quad (38)$$

$$P_{O_2} = \frac{n_{O_2b} V_b}{\Omega T_b} \quad (39)$$

Then Henry's law can be used to get the interface mole fractions for the next time advance of Eqs. (30) and (31). Modifying Eqs. (22) and (23), we get

$$x_{H_2B} = \frac{P_{H_2}}{\Gamma_{H_2}} \quad (40)$$

$$x_{O_2B} = \frac{P_{O_2}}{\Gamma_{O_2}} \quad (41)$$

Thus, to advance this EOS for some system pressure P , we advance Eqs. (20) and (21) and evaluate Eqs. (22)-(29). If the threshold for mass diffusion is satisfied, we must instead freeze N_b at N_{bb} , advance Eqs. (30)-(33), find the bubble radius, temperature and total bubble volume by iterating Eqs. (35)-(37), and finally, evaluate Eqs. (38)-(41). In both cases, Eqs. (18) and (19) must also be advanced. The total system volume change must match that given by the hydrodynamics equations for the same system pressure.

Slurry. For the slurry equation of state, we assume most of the fission products deposit their energy in finite sized (order 1 millimeter radius) undissolved spherical ash particulates uniformly mixed in water. We ignore the radiolysis due to fission energy escaping the particulate but include this energy as a source term in the temperature equation for the water. Once the ash particle temperature exceeds the water saturation temperature at the system pressure, vaporization around the particulate begins. The vapor cloud forms a void contributing to reactivity feedback via the first feedback term in Eq. (7). Heat from the particulate also makes its way out to the water providing another source term in the temperature equations for the water. As in the case of the solution, the heating of water causes volume expansion contributing to reactivity feedback via the second feedback term in Eq. (7).

Figure 3 shows the heat transfer processes around each slurry particulate. The heat transfer correlations are taken from the PM-Alpha particulate, vapor, and water heat transfer code, which has been benchmarked extensively against experimental data (Angelini, et al., 1995, Theofanous, et al., 1997).

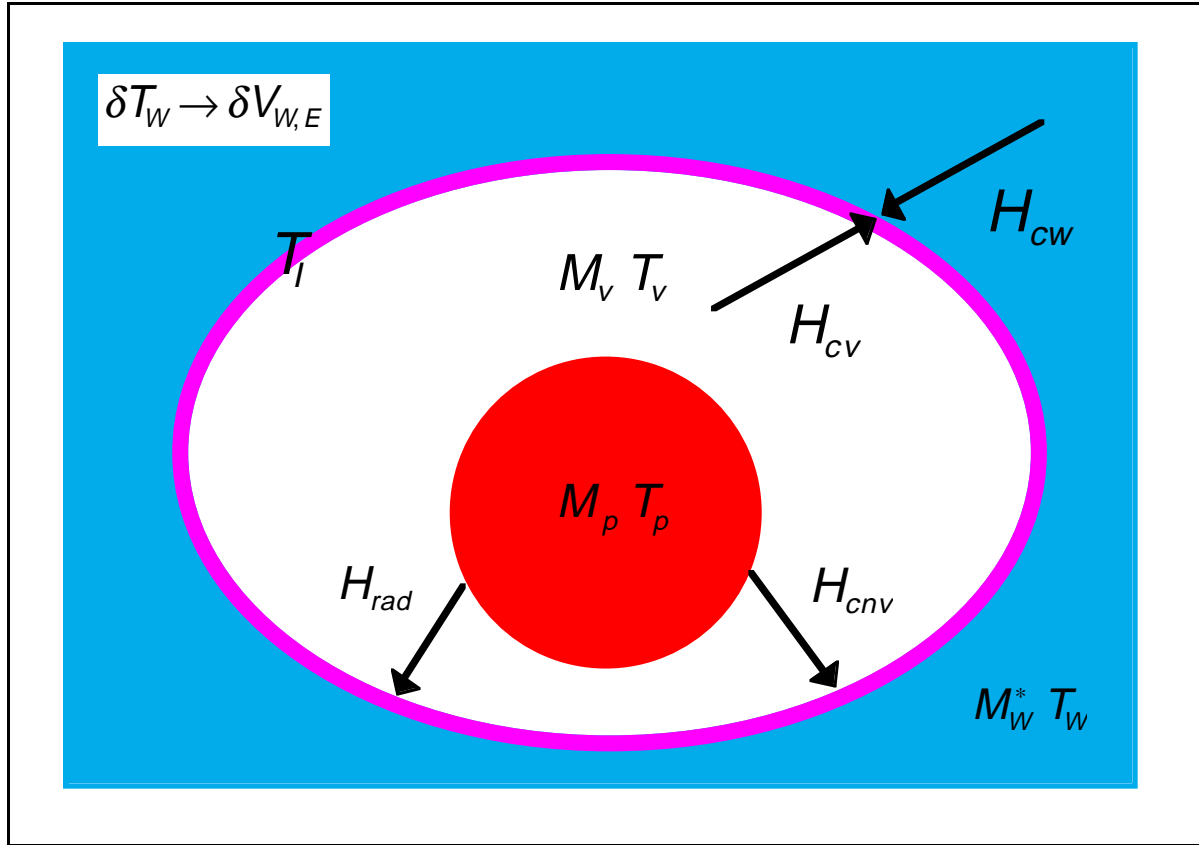


Figure 3: Slurry heat transfer.

Initially, the water is below the saturation temperature and no vapor exists. As the particles heat, eventually the particle surfaces reach the saturation temperature corresponding to the liquid pressure. At this time, vapor begins to form. We consider heat transfer to the vapor water interface. The interface is denoted by the magenta line. Heat transfer from the particulate is by radiation and convection. Heat transfer from the vapor and from the water is by conduction. A fraction g of the fission power is the heat source in each particulate and a fraction $(1-g)$ of the fission power directly heats the surrounding water. Heat dumped to the interface goes into water vaporization with the newly formed vapor retaining the heat as a source term in the vapor temperature equation. By convention, we show heat transfer from the water to the interface, but in reality the heat flows out from the interface as another source for the water temperature equation.

The temperature at the water vapor interface is given by the Clapeyron equation evaluated at the system pressure P :

$$T_l = T_{ref} \left[1 - \chi \log \left(\frac{P}{P_{ref}} \right) \right]^{-1} \tag{42}$$

The reference terms and the χ term are the same as that for Eq. (24).

The energy balance in each particulate is given by

$$M_p C_p \dot{T}_p = \frac{g W_A}{N_p} - A_p (H_{rad} + H_{cnv}) (T_p - T_I) \quad (43)$$

The subscript p stands for particulate. M is the mass, C is the heat capacity, A is the surface area and N_p is the number of particulates which is found by dividing the total ash mass known from the fill phase of the calculation by the particulate ash mass which is the product of the particulate density and volume. The first term on the RHS is the fission source and the second term is the heat escaping from the particulate surface area by conduction and convection.

Equation (43) is valid until the melt temperature is reached. During melt, which occurs at 3120 K for uranium oxide, the temperature is held fixed and the per unit mass internal energy of the particulate is accumulated using the RHS of Eq. (43) until the heat of fusion, 0.285 MJ/kg in uranium oxide, is achieved. Once the phase conversion is completed, Eq. (43) is again advanced. This assumes the liquid particulates have the same heat transfer coefficients. Eventually, either vaporization of the whole particulate or breakup of the particulate while in its liquid form before vaporization would occur but these effects are beyond the scope of this modeling.

The energy balance in the vapor cloud is given by

$$M_v C_{Vv} \dot{T}_v = -P \dot{V}_v - A_v H_{cv} (T_v - T_I) + \dot{M}_v C_w (T_I - T_{w0}) - \dot{M}_v C_{Vv} (T_v - T_I) \quad (44)$$

where C_v is the heat capacity at constant vapor volume and V_v is the vapor volume around each particulate. The first term on the RHS is the work done in expanding the vapor cloud and the second term is the loss of energy from the vapor to the interface by conduction. Both these terms cause the vapor to cool. The third term on the RHS is heat brought in on vaporization, i.e. the energy carried by the liquid water that was heated from the initial water temperature to the interface temperature before vaporization. The fourth term on the RHS is the cooling due to mixing newly created vapor at the interface temperature with the existing vapor at the vapor temperature.

The energy balance in the water adjacent to the vapor cloud is given by

$$M_w^* C_w \dot{T}_w = \frac{(1-g)W_A}{N_p} - P \dot{V}_w^* - A_v H_{cv} (T_w - T_I) - \dot{M}_v C_w (T_I - T_{w0}) \quad (45)$$

The superscript * indicates the portion of water mass or volume associated with each particulate as indicated in Fig. 3, e.g. $M_w^* = M_w / N_p$. The first term on the RHS is the direct fission heating. The second term on the RHS is the work in expanding the water. The third term on the RHS is the conduction to the interface. The fourth term on the RHS is the energy lost due to the vaporization of water brought up to the interface temperature. The first and third RHS terms heat the water while the second and fourth terms cool the water.

The energy directed at the water vapor interface goes into vaporization at the interface temperature:

$$\dot{M}_v h_{vap}(T_I) = A_p (H_{rad} + H_{cnv}) (T_p - T_I) + A_v [H_{cv} (T_v - T_I) + H_{cw} (T_w - T_I)] \quad (46)$$

Adding Eqs. (43), (44), and (45) and substituting Eq. (46) gives the total change in internal energy of each particulate, vapor, and associated water ensemble as a balance of the fission heating and the PdV work and energy absorbed in phase conversion.

Since we are interested in the expansion of the entire system and not just the water associated with each particulate, we multiply Eq. (45) by N_p to get

$$M_w C_w \dot{T}_w = (1-g)W_A - P\dot{V}_w - N_p \left[A_v H_{cw} (T_w - T_I) + \dot{M}_v C_w (T_I - T_{w0}) \right] \quad (47)$$

which in combination with

$$\dot{V}_w = V_w \left(\beta_w \dot{T}_w - \frac{\dot{P}}{K_w} \right) \quad (48)$$

gives the water expansion.

The volume due to *all* of the vapor clouds $V_v = N_p V_v$ is given by the ideal gas law

$$PV_v = \frac{N_p M_v}{\Lambda_w} \Omega T_v \quad (49)$$

The change in water and vapor volumes must match that found by the hydrodynamics for the same system pressure.

Since the vapor mass is so small, solving Eqs. (44) and (46) for some fixed system pressure can be numerically challenging. We first evaluate Eq. (42) to find the interface temperature. Then we evaluate the heat transfer coefficients and vapor surface area using the old time step values of the temperatures. Next, we explicitly advance Eq. (43) to find the particulate temperature. If the particulate temperature is *less* than the interface temperature, we redo the advance on fission power only and then solve Eqs. (47) and (48) for the water temperature and volume, noting that the bracketed term in Eq. (47) does not contribute to the water temperature advance in this situation.

On the other hand, if the particulate temperature is greater than the interface saturation temperature, vaporization is possible. We first explicitly advance the vapor mass Eq. (46). This provides us with M_v but dM_v/dt is folded into a semi implicit advance of Eq. (44) by substituting Eq. (46) and Eq. (49) divided by N_p . Equations (47) and (48) are still solved for the water temperature and volume and Eq. (49) is solved for total vapor volume around all particulates.

We now call out the formulae for the various heat transfer coefficients and detail the vaporization energy and vapor surface area calculation. The radiative heat transfer coefficient is given by

$$H_{rad} = \psi \phi (T_p^2 + T_I^2) (T_p + T_I) \quad (50)$$

where ψ is the emissivity (≈ 0.7), and ϕ is the Stephan Boltzmann constant ($5.67 \times 10^{-8} \text{ W/m}^2 \text{ K}^4$). The convective heat transfer coefficient is given by

$$H_{cnv} = 2.98 \left\{ \frac{U_p M_v K_v \left[h_{vap}(T_I) + 0.68 C_{pv} (T_p - T_I) \right]}{2 V_v R_p (T_p - T_I)} \right\}^{1/2} \quad (51)$$

where C_p is the heat capacity at constant vapor pressure, K_v is the vapor thermal conductivity, U_p is the particulate velocity in the water (order < 1 m/s, depends on hose scenario, etc.), and R_p is the particulate radius. Equation (51) applies if $T_p - T_I > 1000K$. At this temperature difference, film boiling is stable. If the temperature difference is lower, we ignore nucleate boiling convective heat transfer and set $H_{cv} = 0$. The area for both of these heat transfers is given by the particulate surface area $A_p = 4\pi R_p^2$.

The vaporization heat at the interface temperature is the difference between vapor enthalpy at T_I and the water enthalpy at T_I and is given by

$$h_{vap}(T_I) = (h_{v,ref} - h_{w,ref}) + (C_{pv} - C_w)(T_I - T_{ref}) \quad (52)$$

The vapor cloud around the particulate is not spherical due to the particulate velocity in the water. However, as in the case of cubes and spheres, we can write $A_v = 6V_v / L_v$ where the vapor cloud scale length is given by a Weber criteria balancing inertia and surface tension effects:

$$L_v = \frac{8\gamma}{\rho_w U_p^2} \quad (53)$$

Using this scale length, we can now write the conductive heat transfer coefficients from the vapor and water to the interface:

$$H_{cv} = \frac{2K_v}{L_v} \quad (54)$$

$$H_{cw} = \frac{K_w}{L_v} c(2 + 0.6 \text{Re}^{1/2} \text{Pr}^{1/3}) \quad (55)$$

where K_w is the water thermal conductivity, $\text{Re} = \rho_w U_p L_v / \mu_w$, $\text{Pr} = \mu_w C_w / K_w$, and μ_w is the water viscosity. c is a geometrical fit parameter from Angelini which we set to unity.

Comparison to Experiment

CRAC 23. CRAC is a series of criticality excursion experiments carried out by the Commissariat l'Énergie Atomique (CEA) in the early 70s. The experiments consisted of a 15 cm radius tube filled with a solution of uranyl nitrate. Both the concentration of uranyl nitrate and the fill rate were varied to obtain different excursions.

We modeled shot 23 since the fission rate versus time during the first pulse was documented in detail (Lecorche and Seale, 1973). This shot had a 92 g/l solution at fill rate which gave a 0.31 \$/sec insertion rate. We set up nearly identical insertions in our simulation. Since the shot did not start from a stable power level, the initiation delay of Eq. (10) is important. We chose $\delta = 0.8$ to give the experimentally measured 4.6 sec delay from delayed critical ($k=1$, $q=0$) to the fission rate or power peak. For the bubble nucleation radius needed for the solution EOS, we chose 250 nm and used the Norman-Spiegler calculations to infer nucleation lifetime given the radius. The results of the simulation and the experiment are shown on Fig. 4a.

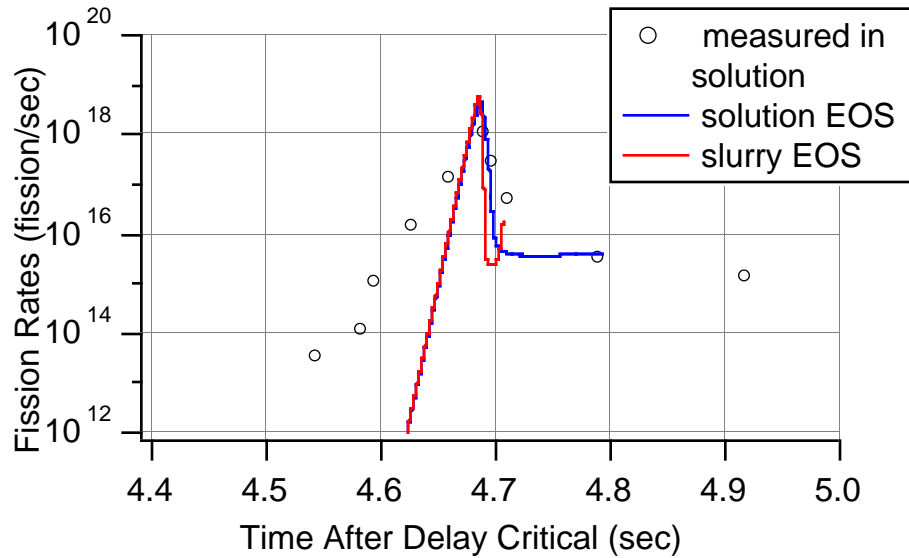


Figure 4a: Comparison of experiment and EOS calculations for CRAC 23 fission rates.

Comparing the blue curve for the solution EOS calculations and the measurements, we see the calculated pulse is quite a bit sharper than the measured pulse, however the total first pulse energy was calculated to be 4.0×10^{16} fissions and measured to be 4.6×10^{16} fissions. Additionally, a water temperature rise was calculated to be 12 K and measured to be about 12 K at the end of the first pulse. No pressure measurements were available but we calculated a peak pressure of 1.2 atm.

The discrepancy in peak shape is most likely due to our simple neutronics model. Note that our power rises rapidly for either EOS long before significant heat can build up to cause expansion and shutdown. It is possible that the simple neutron lifetime as given by Eq. (3) is in error. If the lifetime is longer, the pulse would be less sharp and more in agreement with measurement, but the underlying reason for the discrepancy could be buried in our lack of spatial dependence.

There is also a sensitivity to the choice of bubble nucleation radius. If a bubble nucleation radius less than 100 nm is chosen, the first pulse shuts down only by water thermal expansion and not enough dissolved radiolytic gas builds up in solution to exceed the nucleation threshold of Eq. (29). If this happens, however, the fission rate only drops two orders of magnitude below its peak value which is in clear disagreement with what was measured. A nucleation radius greater than 300 nm allows nucleation to cease and therefore bubble growth and pulse shutdown by void feedback to start too soon. This reduces the power peak but also reduces the total first pulse energy to levels far below what was measured.

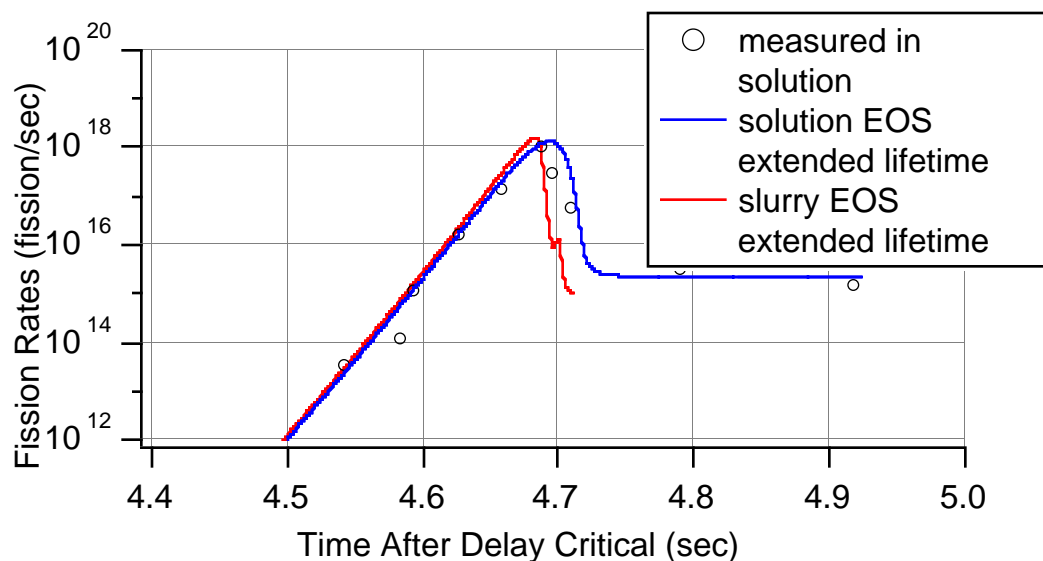


Figure 4b: Comparison of experiment and EOS calculations for CRAC 23 fission rates for tripled neutron lifetime.

We have tripled the neutron lifetime to empirically fit to the experiment and the results are shown on Fig. 4b. We chose $\delta = 0.6$ to give the experimentally measured 4.6 sec delay from delay critical to power peak. The first total pulse energy for this calculation was 4.4×10^{16} fissions and the water temperature and peak pressure did not change significantly.

The red curves in Figs 4 show the calculated power pulse if a slurry EOS is used instead of a solution EOS. We chose a 1 mm particulate radius for this case but kept all fill and initiation conditions the same as in the solution EOS simulation. We use the same neutronics model as used for the solution, neglecting the potential self-shielding in the particles. In this case, the main shutdown mechanism is void formation by vaporization of water due to heat transfer from the particulate. For Fig. 4a, the peak particulate temperature is 2110 K, below melting, but water vapor formation for the slurry EOS occurs faster than water thermal expansion and bubble nucleation and growth for the solution EOS. This results in a peak pressure of 3.6 atm and a faster fission rate drop in the red curve than in the blue curve. For Fig 4b, the peak particulate temperature is 1730 K and the peak pressure is 2.8 atm. In all calculations, a slight delay between peak fission rate and peak pressure was observed due to the inertia of the system.

SILENE S2-173. The SILENE series of criticality excursion tests was also done by CEA following the CRAC series. SILENE is a reactor fueled with a 71 g/l uranyl nitrate solution. The reactor tank is annular with a 3.8 cm inner radius and an 18 cm outer radius. The center contains the burst rod by which an excursion is initiated. During the excursion, the pressure in the tank was monitored to assess pressure transient hazards during an excursion.

We modeled shot S2-173 since time dependent fission rate and pressure data were documented in the available references (Babry, 1987). Recall that our model is based on cylindrical geometry and does not account for burst rods. To model this shot, we chose a cylindrical radius of 17.6 cm to preserve the tank cross sectional area. To start the excursion, we used a fill rate that made the accumulated fissions at the time when the fission rate peaks equal to the measured value of 1.13×10^{17} fissions. This corresponded to a 13 \$/sec insertion rate which is 40 times greater than the

CRAC insertion rate in the previous subsection. Since the reactor is stable before the pulse, i.e. not a subcritical assembly but a steady state reactor, the initiation time is set to be at prompt critical.

For the solution EOS, we chose a bubble nucleation radius of 80 nm and used the Norman-Spiegler calculations to infer nucleation lifetime given the radius. This nucleation radius gave the best pressure data relative to experiment and is on the same order as the 50 nm nucleation radius used in previous calculations of this pulse (Kimpland and Kornreich, 1996). Recall that for the CRAC comparison in the previous subsection, we used a bubble nucleation radius 3 times as large. The choice for the CRAC nucleation radius was motivated by an attempt to match total pulse energy, which itself is an inaccurate calculation due to our simple neutronics model. Nonetheless, it may be that hotter solutions support smaller nucleation radii and the SILENE pulse creates a hotter solution during bubble nucleation than the CRAC pulse because of the higher power levels involved.

Figures 5 and 6 show the fission rate and pressure pulse transients calculated and measured. As in the CRAC case, the solution EOS calculation (blue curve) shows a sharper fission rate pulse shape than measured, although the agreement is better. The solution EOS calculation of the pressure shows a lower and more delayed pulse but with the same general pulse shape. This is in contrast to previous calculations of this pulse (Kimpland and Kornreich, 1996) in which the fission rate shut down occurred more rapidly and the corresponding pressure transient was much sharper and less delayed.

Note that our early time power rise is again fast compared to measurement. The problem was more evident with our CRAC simulations and we suspect an incorrect neutron lifetime estimate. Here, we did not study increased neutron lifetime.

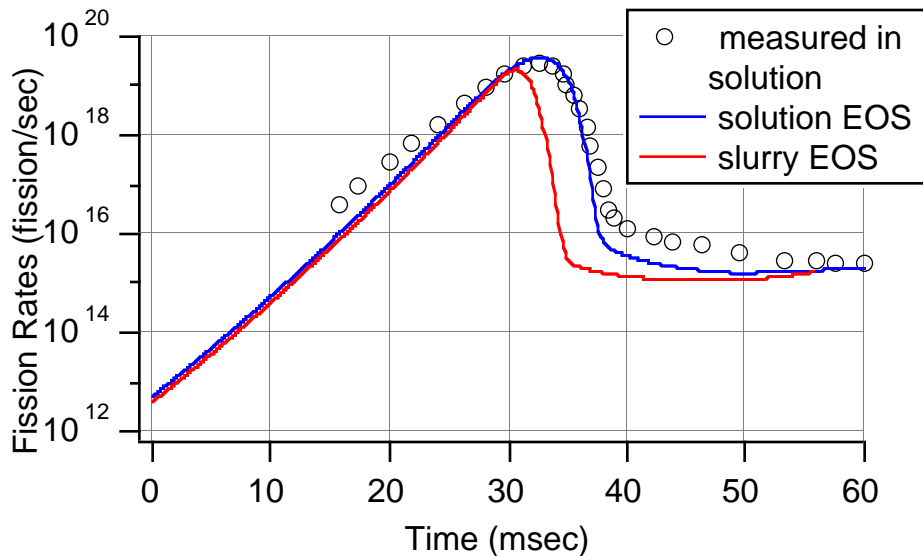


Figure 5: Comparison of experiment and EOS calculations for SILENE S2-173 fission rates.

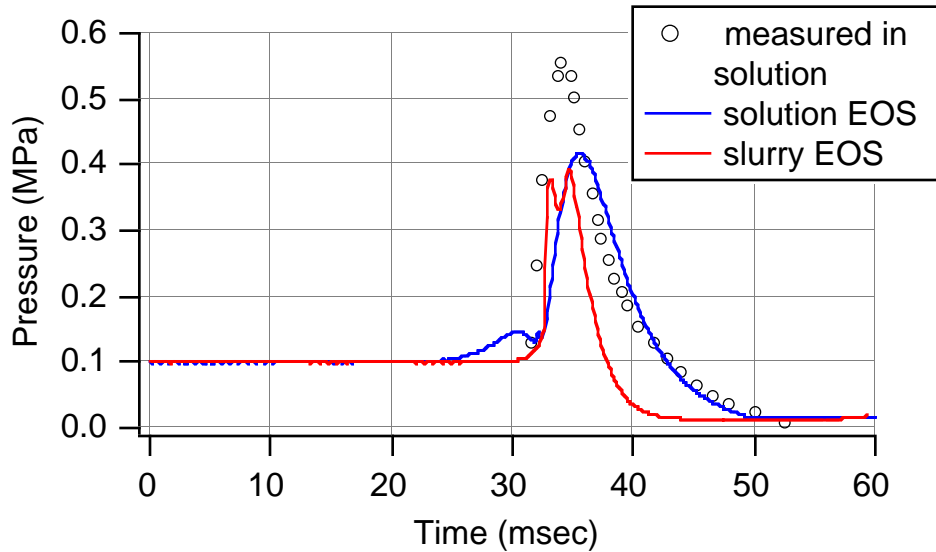


Figure 6: Comparison of experiment and EOS calculations for SILENE S2-173 tank pressures.

The red curves in Figs. 5 and 6 show the same SILENE calculation but with the slurry EOS used instead of the solution EOS. The particulate radius was 1 mm. For this pulse, the particulate temperature exceeded melt and enough energy was in the pulse to exceed the heat of melting and allow additional slight temperature rise of the resulting particulate droplet. Temperature required for particulate droplet vaporization was not approached.

The notches in the pressure curve in Fig. 6 are due to the relative timing of water thermal expansion and void expansion. In both cases, as the excursion proceeds, heat dumped directly into the water causes thermal expansion which slows but does not stop the excursion. During the expansion, the system pressure rises slightly. When the excursion slows, heat dumped into the water slows, which causes the system pressure to drop again. However, the reduced expansion coupled with the continuing reactivity insertion causes the excursion to continue until the dominant void feedback mechanism for both EOS finally shuts down the excursion.

In Fig. 5, note the faster shutdown for the slurry EOS and in Fig. 6, note the earlier and sharper pressure peak for the slurry EOS. For the slurry EOS, there are 7.73×10^{16} first pulse fissions and for the solution EOS, there are 1.99×10^{17} first pulse fissions. The slurry EOS pressure peaks at 3.9 atm and the solution EOS pressure peaks at 4.2 atm. The pressures peaks are comparable even though the slurry EOS first pulse energy is a factor of 2.6 lower than the solution EOS first pulse energy.

The main shutdown mechanism for the solution EOS calculation is bubble growth after nucleation ceases. The main shutdown mechanism for the slurry EOS is water vapor cloud formation and expansion around the particulate. All that is required for the onset of water vaporization is the particulate temperature to exceed the saturation temperature. Then, on the time scale of the fission pulse, the particulate temperature exceeds the saturation temperature by an amount large enough that radiant heat transfer leads a significant vaporization volume. The greater delay in shutdown for the solution EOS stems mainly from the time required to build up enough dissolved radiolytic gas to exceed the nucleation threshold. Once the threshold is exceeded, the bubble growth rate provides a total void growth rate and volume roughly similar to that of vapor cloud formation and expansion. Both EOS's show an inertial lag between power and pressure

peaks, but inertia only slows and does not delay void feedback shutdown. In summary, the solution excursion tends to release less kinetic energy per unit fission energy than a slurry.

Fire Hose Slurry Response

Here, we model the excursions due to mixing of fire hose water at 150 GPM and 1500 GPM to a fixed 3 kg mass of uranium oxide ash. The results *should only be considered extremely gross yield estimates* for a variety of neutronic and hydrodynamic reasons:

- For the case of excursions faster than the sound transit time across the assembly, the lack of spatial dependence in the model could lead to short disassembly times since expansion is the same for all locations in the accounting for the shock transit time delays. Shock waves can also lead to recollapsed vapor clouds.
- For lack of proper uranium oxide neutronic data varying from very high to very low concentrations experience as the water mixes with the initially dry ash, we use the uranyl nitrate data that is really only good for concentrations at or below 200 g/l.
- Doppler broadening feedback as well as possible inhomogeneity (self-shielding) effects are missing.
- The excursions show that particulate temperatures can lead to particulate vaporization even at the high system pressures achieved. On the way to full vaporization, the melted particulate droplets can subdivide.
- For 1500 GPM, the calculated pressures are well above the 22.1 MPa critical pressure for water. At these pressures, we never have a liquid and vapor phase existing in equilibrium and the basis for the slurry EOS is lost.

The hope is that incorporation of the EOS into more sophisticated neutronic-hydrodynamic codes will capture some of these effects, however, experimental validation will be required.

The purpose of this section is to show trends in fission yield and pressure peak for different mixing rates, sump radius and particulate sizes. Figure 7, shows, for both 150 GPM and 1500 GPM mixing, the effect of particulate radius on the excursion for a fixed sump radius of 20 cm. The “sump” in this case is really a cylindrical tank in which the ash and water can mix. For all of these simulations a $\delta = 1$ initiation delay is used.

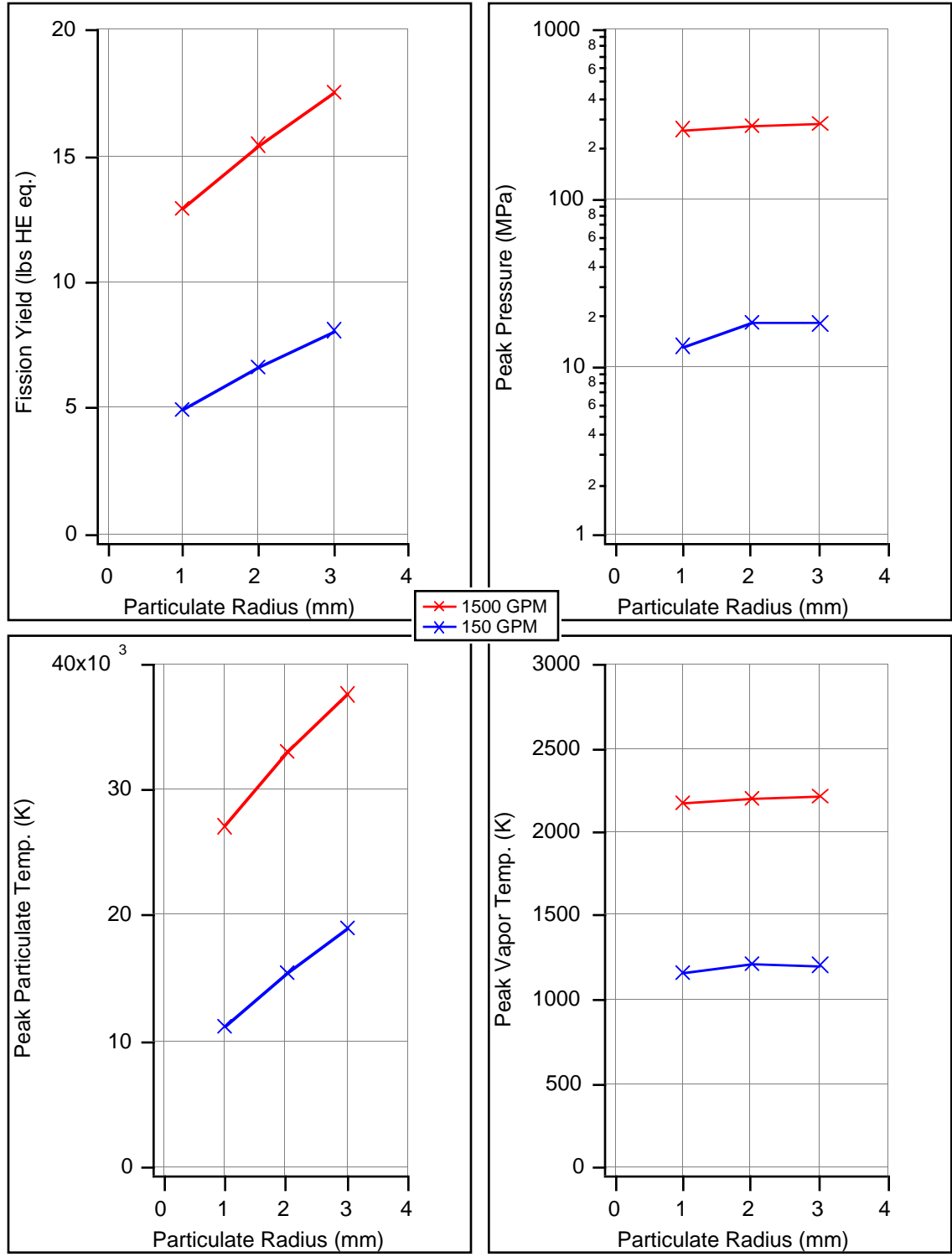


Figure 7: Excursion output for varying particulate size at a 20 cm sump radius.

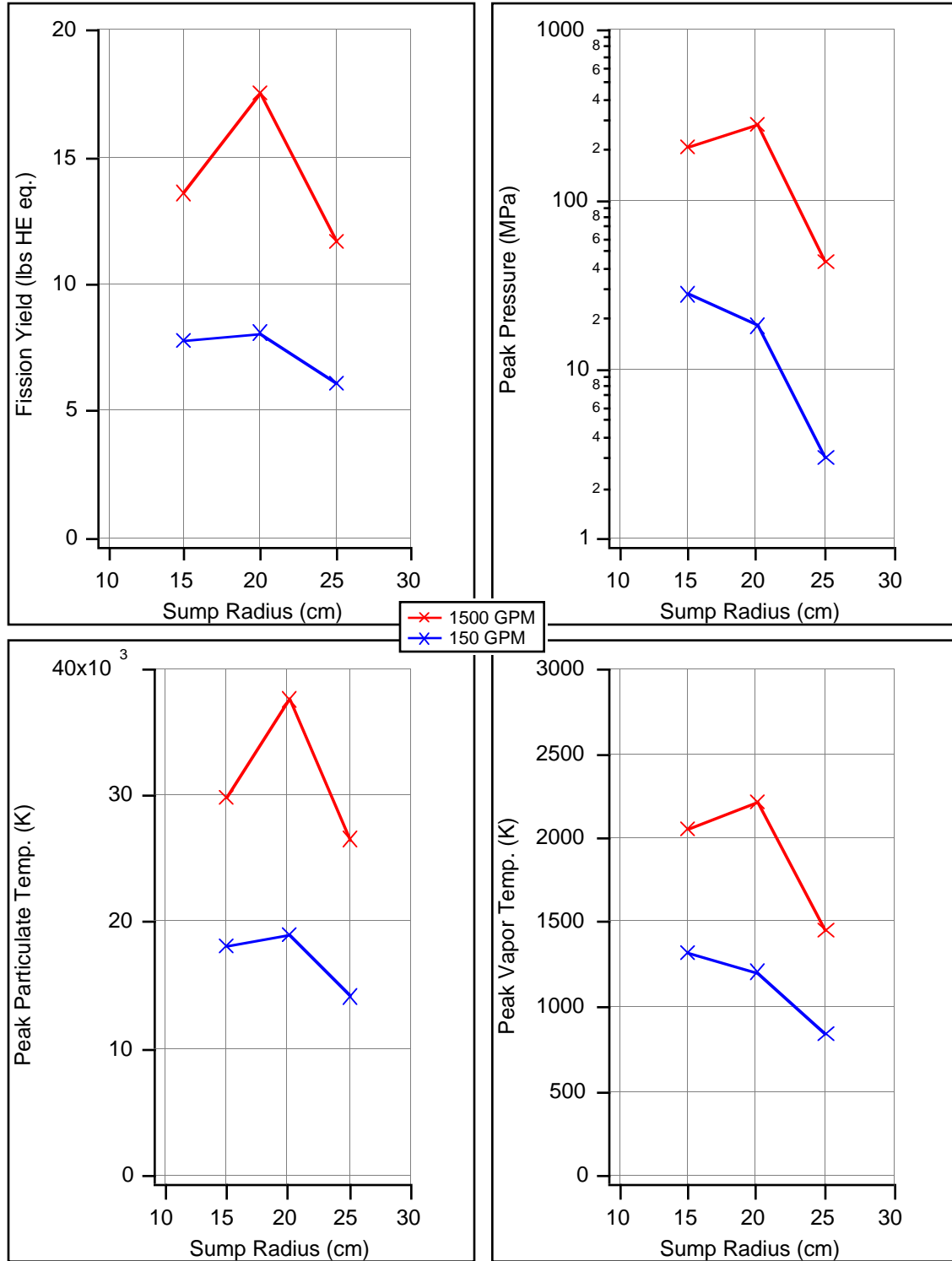


Figure 8: Excursion output for varying sump radius at a 3 mm particulate radius.

The general trends indicate a greater output with increasing particulate radius. For a fixed ash mass, the particulate surface area for heat transfer is inversely proportional to the particulate radius. This limits heat transfer out of the particulate and therefore reduces the excursion shutdown. An

order of magnitude increase in mixing rates, and therefore reactivity insertion rates, results in less than an order of magnitude increase in output since output is proportional to total fast reactivity insertion which is roughly equal to the insertion rate times the delay time. This product goes as the square root of the insertion rate.

The first pulse fission yields range from about 5 lbs. HE equivalent to nearly 20 lbs. HE equivalent, where 1 fission = 1.37×10^{-17} lb. HE. equ. The peak pressures range from 100s to 1000s of atmospheres which in combination with the yields, can represent a significant hazard. Eventhough water vapor formation gives a faster than expected shut down and thus reduced yields, strong sharp pressures result from faster shutdowns. Note that in all cases, particulate vaporization is expected and water vapor temperatures are consistent with achieved pressures. Figure 8 shows similar results except sump radius is varied for a fixed 3 mm particulate radius. The same general levels of output and trends with mixing rate are produced. Note that there is a maximization of output around the 20 cm sump radius.

The few lbs. HE equivalent calculated here are in order of magnitude agreement with previous estimates for slurry output *if it is assumed in these estimates that shutdown occurs at the onset of vaporization* (Kruger, 1993). However, Kruger assumed that disassembly and shutdown does not occur until one cross-slurry sound transit time, increasing the yield a few orders of magnitude. In reality, the complications noted in this report make simple predictions of yield difficult. In our calculations, we find that particulate melt occurs within a millisecond before peak power is reached. Thus, the effects of particulate phase conversion and mixing with vapor will play a role in the neutronics beyond simple void formation and volume expansion feedback.

The first improvement to the slurry EOS is a particulate vaporization model which would work as follows. As the problem proceeds, we would check to see if the particulate temperature reaches the vaporization temperature at the current system pressure. If vaporization is reached, the particulate droplet will be held at the vaporization temperature. The accumulated internal energy per unit mass divided by the required vaporization energy per unit mass evaluated at the system pressure will give the mass fraction of the particulate droplet that has vaporized. The uranium oxide vapor will be treated as an ideal gas and its expansion volume will contribute to the void volume. Once all of the droplet has vaporized, particulate heat transfer will cease and some mix model would be needed.

This addition to the EOS should have two competing effects. The first is that if the particulate temperature can only reach the vaporization temperature, then radiant heat transfer to the liquid water surface will be diminished reducing the amount of water vapor. On the other hand, uranium oxide vapor will be formed. It is unknown how this will effect the rate of formation for the void volume and subsequent shutdown. If the pressure continues to exceed the water critical pressure, yet another EOS would be required.

Conclusion

Our first task for the following fiscal year will be to implement a vaporization model as outlined in the last section. Another slurry EOS addition would be a treatment of melted particulate break-up. Because the pressures calculated approach and in some cases exceed the critical pressure for water, a more detailed water equation of state must be used, rather than the simple analytic forms used here. Next, an incorporation of the EOS into a one or two dimensional neutronics-hydrodynamics code is required. Existing and available design codes and/or reactor codes could be used for this purpose. Finally, more attention should be given to the problem of particulate mixing and suspension for various fire fighting scenarios since this is input information for our modeling.

Once the implementation is complete, we can continue analysis of possible criticality excursions during fire-fighting scenarios with a more detailed physics code that would include

spatial dependencies and shock effects. The main problem at this stage would be code validation. An experiment involving fissile particles squirted with high pressure fire hose water is possible, however, regulatory difficulties will be present. An alternative experiment involving hot metal and ceramic particles dumped into water have been conducted to check the PM-Alpha two-phase heat transfer code. We could use these same tests to check the hydrodynamic and EOS sections of our code.

Acknowledgment

The authors wish to thank Hans Kruger and Roger Speed for bringing this problem to the attention of the safety community. This work was done under the auspices of the United States Department of Energy by Lawrence Livermore National Laboratory and the University of California under contract W-7405-ENG-48.

References

- Speed, R. D., *The Nuclear Criticality Safety Requirement*, Lawrence Livermore National Laboratory, presentation to EIVR-55, (1998).
- Kruger, H. W., *Nuclear Yield from Criticality Excursions in Fissile-Particulate/ Water Mixtures*, Lawrence Livermore National Laboratory, DDV-94-0001 (1993).
- Kimpland, R. H., and Kornreich, D. E., "A Two-Dimensional Multiregion Computer Model for Predicting Nuclear Excursions in Aqueous Homogeneous Solution Assemblies", *Nucl. Sci. and Eng.* **122**, 204 (1996).
- Mee, W. T., Reed, D. A., and Taylor, R. G., *Consequences of a Postulated, Moderated Criticality Accident at the Oak Ridge Y-12 Plant*, Oak Ridge National Laboratory, Y-DD-384, (1988).
- Lecorche, P., and Seale, R. L., *A Review of the Experiments Performed to Determine the Radiological Consequences of a Criticality Accident*, Oak Ridge National Laboratory, Y-CDC-12 (1973).
- Barbry, F., *Review of Pressure Wave Experiments in the SILENE Reactor*, Commissariat le Energie Atomique, Technical Note SRSC No. 87.96 (1987).
- Angelini S., Yuen W. W., and Theofanous T. G., "Premixing-related Behavior of Steam Explosions", *Nuc. Eng. and Design*, **155**, 115 (1995).
- Theofanous T.G., Yuen, W. W., and Angelini, S., *The Verification Basis of the PM-ALPHA Code*, University of California, Santa Barbara, Proceedings, OECD/CSNI Specialist Meeting on FCI, JAERI-Tokai Research Establishment, Japan, (1997).
- Lutz, H. F., *Nuclear Criticality Safety Assessment Calculations: Part I. Calculating Power Histories in Nuclear Excursion*, edited by H. J. Kroopnick, Lawrence Livermore National Laboratory, M-164, (1985).
- Kornreich, D. E., "Reactivity Feedback Mechanisms in Aqueous Fissile Solutions", *Nucl. Sci. and Eng.* **115**, 50(1993).
- Duderstadt, J. J. and Hamilton L. J., *Nuclear Reactor Analysis*, (John Wiley and Sons, New York, 1976), p. 610.
- Norman, A., and Spiegler, P., "Radiation Nucleation of Bubbles in Water", *Nucl. Sci. and Eng.* **16**, 213 (1953).